Hydrogen storage in crystaline structures: STC Team

Stijn Van Vooren, Thomas Salens and Carlos Esteban Mejía Nicolalde

December 2023

Abstract

Hydrogen gas is an important method, but flawed, method of storing energy. Hydrogen bearing crystals have the potential to resolve certain flaws and improve energy density compared to pure hydrogen gas. To this purpose, several simulations were performed on potential crystals making use of density functional theory with the PBE functional, and with the use of pseudopotentials. We started off with experimentally known crystals composing of H, Al, and Na. These crystals were geometrically optimized for cases where the Al and Na atoms are exchanged for B, and Li, Rb, K respectively, this was done including extra crystals which are known to be potentially stable. Afterwards calculations were performed on the stable crystals (which were identified using the convex hull) to evaluate economical factors.

1 Introduction

The storage of hydrogen is an important ongoing problem. Hydrogen is a very practical fuel source. However, the storage of hydrogen in its elemental form is plagued with several issues such as: density, volatility (incredibly flammable and explosive), its tendency to embrittle metals (making storage quite difficult).[1] Storing hydrogen in liquid form would simply swap one problem for another, density is improved, however, we require very low temperatures to achieve this. A potential solution to this predicament is to utilise hydrogen bearing crystals for storage. This is likely to improve density, remove the embrittlement problem, and will most likely be less volatile.

In this paper we explore certain crystal structures for their potential application in the storage of hydrogen. As analytical methods are inaccessible, we resort to numerical methods. For this paper we made use of Quantum espresso, an implementation of density functional theory with usage of pseudo potentials [2]; whereby we made use of the PBE functional.

To this end, convergence testing was performed. Here we investigated the effects of the parameters: k-mesh, ecutrho, and ecutwfc on the precision of the data. As final part calculations were performed for each of the stable crystals to determine the density of hydrogen gas they can hold, how much pressure this would amount to, and the price of the elements utilized in the crystal.

2 Convergence testing

Note that all simulations throughout this paper were done using Quantum ESPRESSO [3], using a PBE functional and pseudopotentials from the SSSP library [2]. In addition, all CIF files were obtained from materials project [4]. Before embarking on the geometrical optimization of the crystals in question, it is imperative to conduct convergence tests, aimed at determining the optimal values for the k-mesh, ecutwfc and ecutrho, ensuring to obtain the desired precision in the simulations. Ecutwfc and ecutrho correspond to the cutoff energies for wave functions and charge densities respectively. In this study, Tier 1 Hortense HPC [5] has been used, allowing for a practically unrestricted allocation of resources and a high level of accuracy. Our approach involved selecting the most error-prone parameters within these systems namely the total energy E, the total isothermal pressure P, stress tensor τ_{xx}, and total force F_{tot}, and crystals exhibiting higher susceptibility to errors, while still having manageable computational times, namely $NaAlH_4$, $LiBH_4$,

$RbBH_4$ and KBH_4 (all of symmetry group $I4_1/a$). A comparative analysis was conducted for these quantities and crystals, systematically varying the values of k-mesh, ecutwfc, and ecutrho to determine their impact on the selected quantities. For each parameter, the error is computed relative to a reference scenario utilizing significantly high values, considered practically as an exact solution within the limitations of our approximations, i.e. a k-mesh of $20 \times 20 \times 20$, ecutwfc=400, and ecutrho=1600. Throughout the convergence testing process, a consistent trend emerged: the error diminishes as the sizes of k-mesh, ecutwfc, and ecutrho increases. In Table 1 some critical values of these quantities are listed for the $NaAlH_4$ case, while in Table 2 their respective errors are displayed. The other convergence tests yield similar results, but with even

K-Mesh	ecutwfc	ecutrho	E (Ry)	P (kbar)	τ_{xx} (Ry/bohr^3)	F_{tot} (Ry/au)
$10 \times 10 \times 10$	200	800	-279.14929980	13.76	9.696e-5	0.012803
$11 \times 11 \times 11$	250	1000	-279.14946766	13.84	9.752e-5	0.012802
$20 \times 20 \times 20$	400	1600	-279.14959619	13.79	9.716e-5	0.012803

Table 1: Convergence test $NaAlH_4$.

K-Mesh	ecutwfc	ecutrho	E (Ry)	P (kbar)	τ_{xx} (Ry/bohr^3)	F_{tot} (Ry/au)
$10 \times 10 \times 10$	200	800	-2.9639e-4	0.03	7.2e-7	0
$11 \times 11 \times 11$	250	1000	-1.2853e-4	-0.05	1.6e-7	e-6

Table 2: Errors $NaAlH_4$ compared to the $20 \times 20 \times 20$ k-mesh, ecutwfc=400 and ecutrho=1600 case.

lower errors. For a k-mesh of $10 \times 10 \times 10$, ecutwfc=200 and ecutrho=800, the largest errors out of all tested crystals on the quantities of interest read $E_{err} = 2.96e^{-4}Ry$, $P_{err} = 0.03kbar$, $\tau_{xx,err} = 7.2e^{-7}Ry/bohr^3$ and $F_{\text{tot},err} = 1.4e^{-5}Ry/au$. In the remaining of the paper, all simulations use a k-mesh of $10 \times 10 \times 10$, ecutwfc=200 and ecutrho=800. Some critical values of the other convergence tests are displayed in Appendix A Tables 4-9.

3 Phase diagrams

In this section the obtained phase diagrams are discussed, determining the possible stability of all crystals in question. Throughout this chapter, all CIF files were obtained from materials project [4] and geometry optimization has been done using Quantum ESPRESSO VC-RELAX [6]. In the Quantum ESPRESSO VC-RELAX computations, the settings comprised ion dynamics using the BFGS algorithm and cell dynamics employing the BFGS method, with a specified pressure of 0 and a convergence threshold for pressure of 0.1. Throughout all simulations a k-mesh of $10 \times 10 \times 10$, ecutwfc=200 and ecutrho=800 has been utilized.

3.1 Na-Al-H phase diagram

Formation energies of the involved crystals or computed relative to the most stable pure states of their constituents. As pure states we considered the cubic Na(mp-1186081, $\bar{I}$43m), cubic Al(mp-134, Fm3$\bar{m}$) and hexagonal H_2(mp-24504,P6$_3$/mmc). Each of these pure states have been geometry optimized. Furthermore, the crystals cubic NaH(mp-23870, F$\bar{m}$3m), monoclinic Na_3AlH_6(mp-23705, P2$_1$/c), tetragonal $Na_5Al_3H_14$(mp-24822, P4/mnc), tetragonal $NaAlH_4$(mp-23704, I4$_1$/a) and cubic AlH_3(mp-1106356, F$\bar{d}$3m) have been geometrically optimized. From their total energies and the total energies of the geometry optimized pure states, the formation energies were computed, as displayed in the phase diagram along the NaH-AlH_3 line in Figure 1, where the convex hull is drawn by the black lines. In Figure 1, one observes that all crystals have negative formation energy and lie on the convex hull. Meaning they are all potentially stable. Note that these crystals comprise the convex hull in accordance with materials project [4].

3.2 Li-B-H phase diagram

A similar analysis has been done as for the Na-Al-H phase diagram, but this time for some made up crystals. Essentially, the crystal structures cubic NaH(mp-23870, F$\bar{m}$3m), monoclinic Na_3AlH_6(mp-23705, P2$_1$/c),

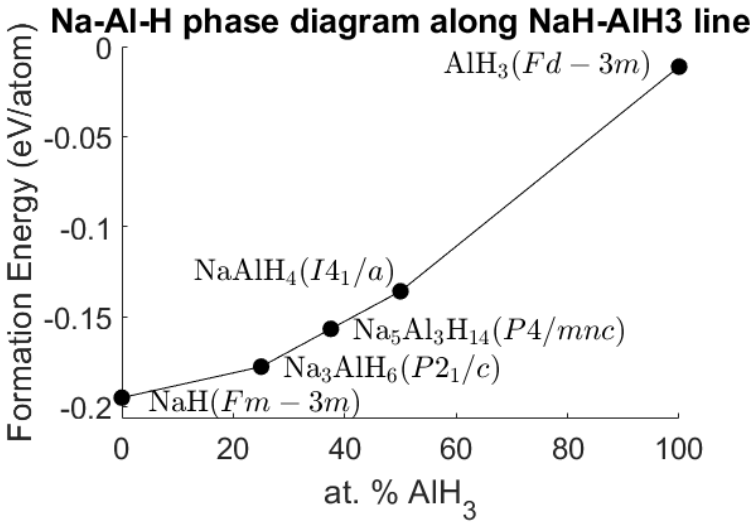

Figure 1: Na-Al-H phase diagram along $NaH\text{-}AlH_3$ line.

tetragonal $Na_5Al_3H_14$(mp-24822, P4/mnc),tetragonal $NaAlH_4$(mp-23704, $I4_1/a$) and cubic AlH_3(mp-1106356, $Fd\bar{3}m$) are taken with the substitution of Na $\rightarrow$ Li and Al $\rightarrow$ B. As pure crystal states trigonal Li(mp-1018134, $R\bar{3}m$), trigonal B(mp-160, $R\bar{3}m$) and hexagonal H_2(mp-24504,$P6_3/mmc$) were considered. Additionally, inspired by the convex hull as given by materials project [8], the two extra crystals orthorhombic $LiBH_4$(mp-1192133, Pnma) and monoclinic BH_3(mp-634117, $P2_1/c$) were geometrically optimized. The obtained phase diagram along the $LiH\text{-}BH_3$ line for all of these crystals is depicted in Figure 2, where the black line corresponds to the convex hull. From Figure 2, we conclude that the convex hull comprises only three potentially

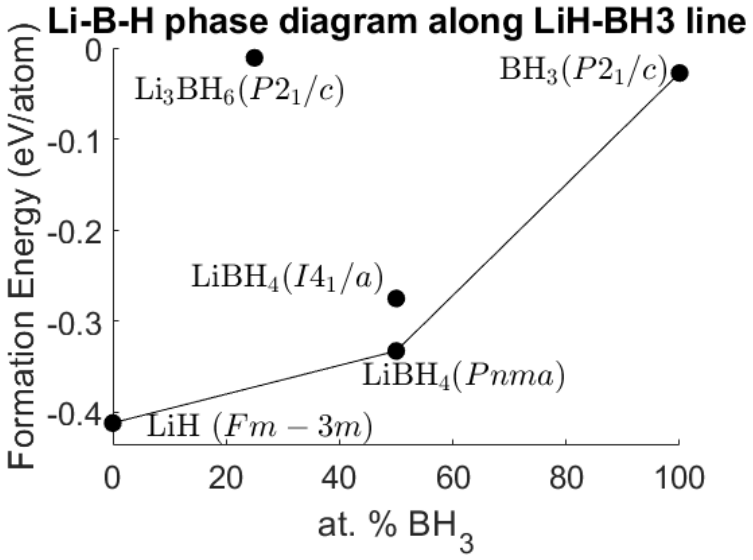

Figure 2: Li-B-H phase diagram along $LiH\text{-}BH_3$ line for all made up crystals and the two additional crystals. All crystals that aren't present on the figure have positive formation energies.

stable crystals while all others are unstable, by either having a positive formation energy or lying above the convex hull.

3.3 Rb-B-H phase diagram

A similar analysis has been done as for the Na-Al-H phase diagram, again for some made up crystals. Essentially, the crystal structures cubic NaH(mp-23870, F$\bar{m}$3m), monoclinic Na_3AlH_6(mp-23705, $P2_1/c$), tetragonal $Na_5Al_3H_14$(mp-24822, P4/mnc), tetragonal $NaAlH_4$(mp-23704, $I4_1/a$) and cubic AlH_3(mp-1106356, F$\bar{d}$3m) are taken with the substitution of Na $\rightarrow$ Rb and Al $\rightarrow$ B. As pure crystal states cubic Rb(mp-70,Im$\bar{3}$m), trigonal B(mp-160, R$\bar{3}$m) and hexagonal H_2(mp-24504,$P6_3/mmc$) were considered. Additionally, inspired by the convex hull as given by materials project [4], the two extra crystals cubic $RbBH_4$(mp-1219553 and BH_3(mp-634117, $P2_1/c$) were geometrically optimized. The obtained phase diagram along the RbH-BH_3 line for all of these crystals is depicted in Figure 5 in Appendix A, where the black line corresponds to the convex hull. Essentially, all formation energies of the made up crystals are positive, and thus unstable, except for RbH(Fm-3m). The convex hull comprises three potentially stable crystals RbH(Fm-3m), $RbBH_4$(mp-1219553 and BH_3(mp-634117, $P2_1/c$).

3.4 K-B-H phase diagram

A similar analysis has been done as for the K-B-H phase diagram, but this time for some made up crystals. Essentially, again, the crystal structures cubic NaH(mp-23870, F$\bar{m}$3m), monoclinic Na_3AlH_6(mp-23705, $P2_1/c$), tetragonal $Na_5Al_3H_14$(mp-24822, P4/mnc), tetragonal $NaAlH_4$(mp-23704, $I4_1/a$) and cubic AlH_3(mp-1106356, F$\bar{d}$3m) are taken with the substitution of Na $\rightarrow$ K and Al $\rightarrow$ B. As pure crystal states cubic K(mp-1184905, $P4_1\bar{3}2$), trigonal B(mp-160, R$\bar{3}$m) and hexagonal H_2(mp-24504,$P6_3/mmc$) were considered. Additionally,inspired by the convex hull as given by materials project [4], the two extra crystals tetragonal KBH_4(mp-37722, $P4_2/nmc$) and monoclinic BH_3(mp-634117, $P2_1/c$) were geometrically optimized. The obtained phase diagram along the KH-BH_3 line for all of these crystals is depicted in Figure 6 in Appendix A, where the black line corresponds to the convex hull. Essentially, all formation energies of the made up crystals are positive, and thus unstable, except for KH(Fm-3m). The convex hull comprises three potentially stable crystals cubic KH(Fm-3m), tetragonal KBH_4(mp-37722, $P4_2/nmc$) and monoclinic BH_3(mp-634117, $P2_1/c$).

4 Hydrogen density

As previously mentioned, our objective is to achieve a efficient method for storing hydrogen, for this purpose, the stability of various crystals were evaluated using phase diagrams.
The analysis of previous section provides us the possibly stable crystals cubic NaH(mp-23870, F$\bar{m}$3m), monoclinic Na_3AlH_6(mp-23705, $P2_1/c$), tetragonal $Na_5Al_3H_14$(mp-24822, P4/mnc), tetragonal $NaAlH_4$(mp-23704, $I4_1/a$), cubic AlH_3(mp-1106356,Fd-3m), cubic LiH(F$\bar{m}$3m), orthorhombic $LiBH_4$(mp-1192133, Pnma), monoclinic BH_3(mp-634117, $P2_1/c$), RbH(Fm-3m), $RbBH_4$(mp-1219553, BH_3(mp-634117, $P2_1/c$), cubic KH(F$\bar{m}$3m), KBH_4(mp-37722, $P4_2/nmc$) and monoclinic BH_3(mp-634117, $P2_1/c$). Out of these possibly stable states, determining the most optimal option remains a crucial aspect. A goal of this section is to decide which crystals have the highest hydrogen gas density (ρ) along with the required gas pressure (P).
The assumption was made that H_2 behaves similarly to an ideal gas, allowing the utilization of the ideal gas equation for idealised pressure and density[7]. The focus remains on attempting to store as much hydrogen as feasible, particularly at room temperature for ease of handling, although convergence and optimization were performed at 0K. Initially, the correlation between pressure and volume is examined Figure 3, followed by an exploration of how density changes concerning pressure Figure 4.

One might consider options like $Na_5Al_3H_14$ or Na_3AlH_6, which contain more hydrogen and exhibit larger volumes, yet maintain relatively lower pressures compared to others, with intermediate density values. However, due to their complex nature, extracting hydrogen from these compounds would involve more intricate processes that might prove less cost-effective in the long term.

LiH, NaH, and KH exhibit the highest hydrogen density, making them strong candidates for efficient storage due to their capacity to store more hydrogen in a smaller volume. However, their smaller volume also implies a higher densities, which could pose a potential risk. Extraction processes from these compounds might be

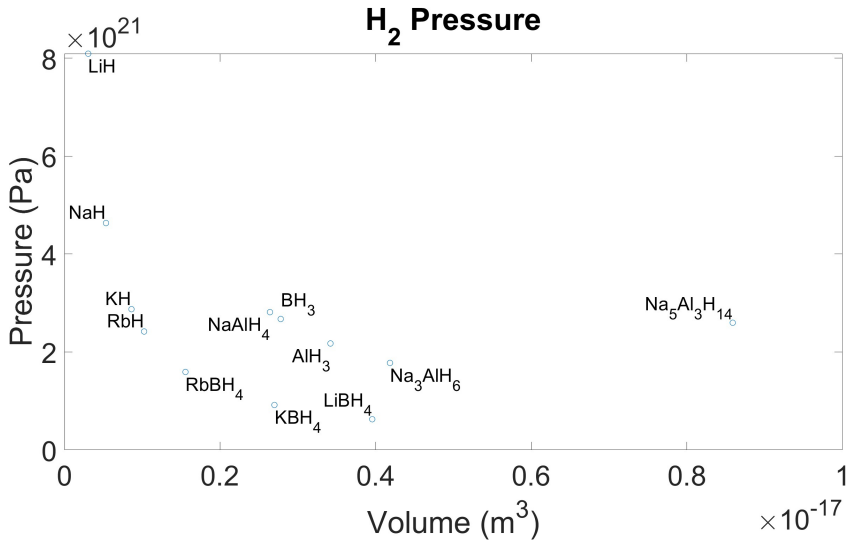

Figure 3: V-P

hazardous, requiring specialized storage devices to prevent leakage risks associated with high pressures. Considering crystals with intermediate properties could be an option, yet given the availability of others with superior characteristics, investing time and resources in these intermediate options might not be the most efficient choice.

The search for effective hydrogen utilization has intensified in recent decades as it remains a key element in the pursuit of clean and renewable energy. Therefore, finding a cost-effective and secure method for its storage is of utmost importance. Let's delve into the potential costs associated with crystals having a higher density of hydrogen LiH, NaH, KH, and $NaAlH_4$.

crystal	**prices (USD/mol)[8]**
LiH	0.69139652
NaH	0.11567036
KH	0.73608395
$NaAlH_4$	0.5823356

Table 3: economical costs

It appears that these crystals are not excessively expensive, indicating potential cost savings by utilizing them. Notably, despite KH having a higher hydrogen density compared to $NaAlH_4$, its cost is higher due to present prices, given that K is more expensive than sodium Na and Al.

5 Conclusion

Conducting stability assessments of various crystals using quantum espresso to perform DFT calculations involved employing convergence tests to get precise data while the computational resources was been kept low. Exploration of different alkaline crystals and alternation between Al and B identified several stable options. Notably, LiH, NaH, KH, and $NaAlH_4$ showed the highest hydrogen density at room temperature. Estimating potential costs associated with their use, we envisioned these crystals as potential future hydrogen storage solutions based on current market prices.

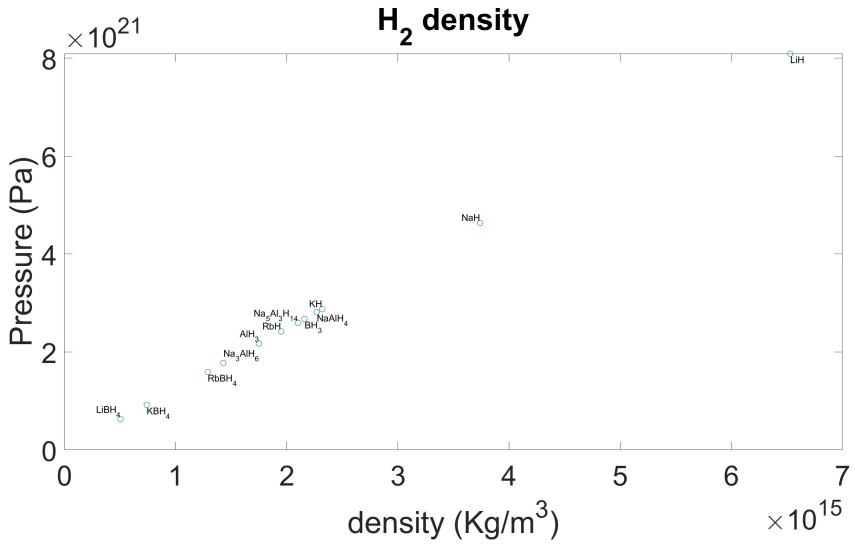

Figure 4: ρ-P

A Appendix

K-Mesh	ecutwfc	ecutrho	E (Ry)	P (kbar)	τ_{xx} (Ry/bohr^3)	F_{tot} (Ry/au)
$10 \times 10 \times 10$	200	800	-50.73141971	-180.48	-1.35381e-3	0.320564
$11 \times 11 \times 11$	250	1000	-50.73143647	-180.49	-1.35387e-3	0.320563
$20 \times 20 \times 20$	400	1600	-50.73145181	-180.48	-1.35379e-3	0.320578

Table 4: Convergence test $LiBH_4$.

K-Mesh	ecutwfc	ecutrho	E (Ry)	P (kbar)	τ_{xx} (Ry/bohr^3)	F_{tot} (Ry/au)
$10 \times 10 \times 10$	200	800	-3.21e-5	0	2e-8	1.4e-5
$11 \times 11 \times 11$	250	1000	-1.534e-5	-0.01	8e-8	1.5e-5

Table 5: Errors $LiBH_4$ to the $20 \times 20 \times 20$ k-mesh, ecutwfc=400 and ecutrho=1600 case.

K-Mesh	ecutwfc	ecutrho	E (Ry)	P (kbar)	τ_{xx} (Ry/bohr^3)	F_{tot} (Ry/au)
$10 \times 10 \times 10$	200	800	-119.59958320	-66.08	-0.00060659	0.429928
$11 \times 11 \times 11$	250	1000	-119.59958513	-66.07	-0.00060659	0.429927
$20 \times 20 \times 20$	400	1600	-119.59959037	-66.07	-0.00060657	0.429928

Table 6: Convergence test $RbBH_4$.

K-Mesh	ecutwfc	ecutrho	E (Ry)	P (kbar)	τ_{xx} (Ry/bohr^3)	F_{tot} (Ry/au)
$10 \times 10 \times 10$	200	800	-7.17e-6	0.01	2e-8	0
$11 \times 11 \times 11$	250	1000	-5.24e-6	0	2e-8	e-6

Table 7: Errors $RbBH_4$ compared to the $20 \times 20 \times 20$ k-mesh, ecutwfc=400 and ecutrho=1600 case.

K-Mesh	ecutwfc	ecutrho	E (Ry)	P (kbar)	τ_{xx} (Ry/bohr^3)	F_{tot} (Ry/au)
$10 \times 10 \times 10$	200	800	-247.84277760	-103.78	-8.6592e-4	0.399945
$11 \times 11 \times 11$	250	1000	-247.84278957	-103.78	-8.6594e-4	0.399945
$20 \times 20 \times 20$	400	1600	-247.84280446	-103.77	-8.6589e-4	0.399949

Table 8: Convergence test KBH_4.

K-Mesh	ecutwfc	ecutrho	E (Ry)	P (kbar)	τ_{xx} (Ry/bohr^3)	F_{tot} (Ry/au)
$10 \times 10 \times 10$	200	800	-2.685999e-5	0.01	3e-8	4e-6
$11 \times 11 \times 11$	250	1000	-1.488999e-5	0.01	5e-8	4e-6

Table 9: Errors KBH_4 compared to the $20 \times 20 \times 20$ k-mesh, ecutwfc=400 and ecutrho=1600 case.

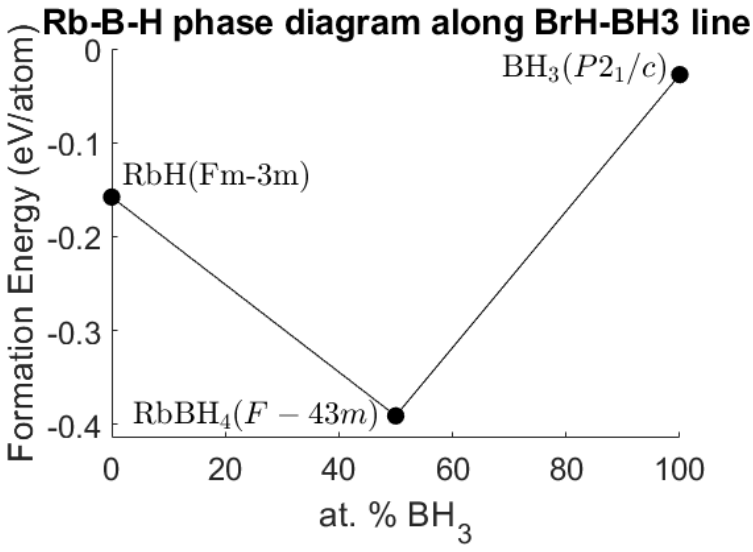

Figure 5: Rb-B-H phase diagram along RbH-BH_3 line for all made up crystals and the two additional crystals. All crystals that aren't present on the figure have positive formation energies.

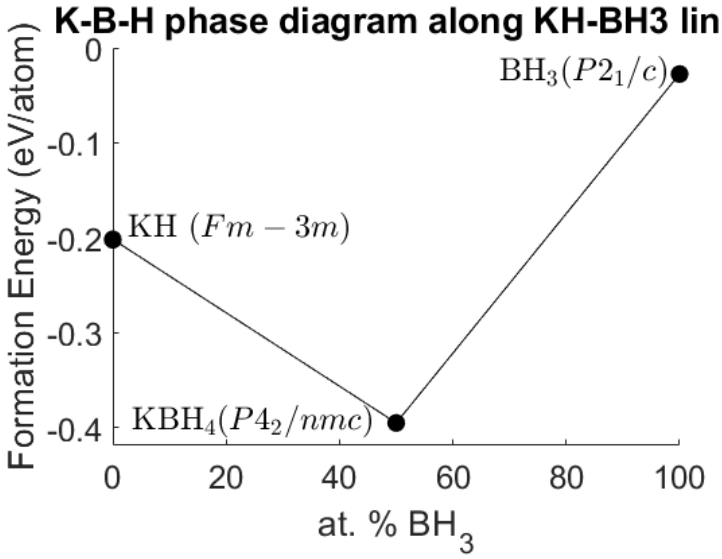

Figure 6: K-B-H phase diagram along KH-BH_3 line for all made up crystals and the two additional crystals. All crystals that aren't present on the figure have positive formation energies.

References

[1] Wikipedia contributors. (2023a, November 20). *Hydrogen*. Wikipedia. https://en.wikipedia.org/wiki/Hydrogen

[2] *Pslibrary* 1.0.0:A.DalCorso,Comput.Mater.Sci.95,337(2014). DOI: 10.1016/j.commatsci.2014.07.043, LICENSE: GNU General Public License (version 2 or later). http://www.quantum-espresso.org/pseudopotentials

[3] OQMD — The Open Quantum Materials Database. (n.d.). https://oqmd.org/analysis/phase_diagram/.

[4] Materials Project - Home. (n.d.). Materials Project. https://next-gen.materialsproject.org/

[5] Tier 1 HPC Hortense UGent - https://docs.vscentrum.be/gent/tier1_hortense.html

[6] Quantum ESPRESSO - VC-RELAX - https://pranabdas.github.io/espresso/hands-on/structure-optimization/

[7] Wikipedia contributors. (2023, December 5). *Density*. Wikipedia. https://en.wikipedia.org/wiki/Density

[8] Wikipedia contributors. (2023b, December 3). *Prices of chemical elements*. Wikipedia. https://en.wikipedia.org/wiki/Prices_of_chemical_elements

[9] *GBRV*: K. F. Garrity, J. W. Bennett, K. M. Rabe, and D. Vanderbilt, Comput. Mater. Sci. 81, 446 (2014). DOI: 10.1016/j.commatsci.2013.08.053, LICENSE: GNU General Public License (version 3). http://www.physics.rutgers.edu/gbrv

[10] *SG15*: M. Schlipf and F. Gygi, Comp. Phys. Comm. 196, 36 (2015). DOI: 10.1016/j.cpc.2015.05.011, LICENSE: Creative Commons Attribution-ShareAlike 4.0 International License (CC BY-SA 4.0). http://www.quantum-simulation.org/potentials/sg15_oncv

[11] OQMD — The Open Quantum Materials Database. (n.d.). https://oqmd.org/analysis/phase_diagram/.